RSC Advances

ROYAL SOCIETY OF CHEMISTRY

www.rsc.org/advances

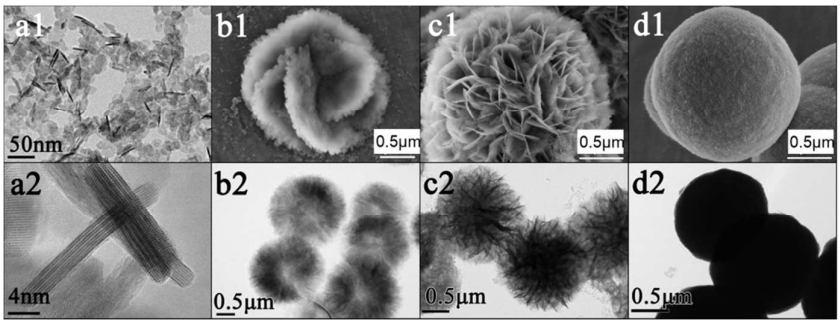

Highly crystallized micro/nano-sized Y_2O_2S and RE(Eu^{3+},Yb^{3+}/Er^{3+}) doped samples were prepared through a one-pot mild (200~250°C) solvothermal synthesis. By simply adjusting the amount of initial sulfur powder, the morphology and assembled structure can be well controlled.

Journal Name

RSCPublishing

ARTICLE

One-pot solvothermal synthesis of singly doped Eu^{3+} and codoped Er^{3+} ,Yb^{3+} heavy rare earth oxysulfide Y_2O_2S nano-aggregates and their luminescence study

Cite this: DOI: 10.1039/x0xx00000x

Received 00th January 2012,
Accepted 00th January 2012

DOI: 10.1039/x0xx00000x

www.rsc.org/

Hong Liu#[a], Pin Liu#[a], Xiangming Su#[a], Jie Liu[a]*, Xiaoqing Li[a], Hongde Luo[a], Zhiling Yao[a], Xibin Yu[a]*, Ming Zhan[b]*

Highly crystallized micro/nano-sized Y_2O_2S and RE (Eu^{3+}, Yb^{3+}/Er^{3+}) doped samples were prepared through one-pot mild (200~250 °C) solvothermal method. By simply adjusting the amount of initial sulfur powder, the morphology and assembled nano-structures could be well controlled. With varying the concentration of sulfur powder from 0.08 M to 0.8M, the morphology and size of the target products varied from 20 nm nanosheests, 2 μm sheet-assembled plates /flowers to 1.5 μm nano-assembled spheres. The luminescent properties of Eu^{3+} doped Y_2O_2S with different morphology were studied. The excitation peak above 300 nm ascribed to S^{2-} - Eu^{3+} charge transfer showed a blue shift of 9 nm compared with bulk sample. When co-doped with Yb^{3+}/Er^{3+}, the Y_2O_2S:Yb^{3+},Er^{3+} nano-aggregates exhibited a tunable emission under 980 nm laser excitation, shifting from greenish-yellow to orange-yellow, with increasing Yb^{3+}/Er^{3+} ratio.

1 Introduction

Due to the high absorption of UV light and efficient energy transfer, high thermal and chemical stability, rare earth oxysulfides have been extensively used as optical functional materials. Among these materials, Rare earth ions-activated Y_2O_2S have been used in many applications. Eu^{3+} ion doped Y_2O_2S is one of the most efficient phosphor that used in the field of color television tubes,[1] long-lasting phosphor,[2] filed emission display[3] and photocatalysis.[4] Y_2O_2S is also an efficient upconversion host for Yb^{3+}/Er^{3+}, Yb^{3+}/Tm^{3+}, Yb^{3+}/Ho^{3+}.

Recently, there is much interest in nano crystalline rare earth oxysulfides synthesized through soft chemical method because of the unique luminescence and magnetics properties resulting from nano size and surface effect.[5-8] As we know, it is difficult to obtain lanthanide oxysulfides directly through some soft synthetic method such as hydrothermal reaction and precipitation, especially for the heavy RE element such as yttrium, because the hard Lewis acid Ln^{3+} doesn't preferentially bind to the soft Lewis base S^{2-}.[9] In the previous references, some light and middle RE oxysulfides can be synthesized through the thermolysis method in high-boiling-point organic solvent.[10] However, according to the density functional theory calculation results, from light rare earth to heavy rare earth, the thermo-dynamical stability are being lower, higher chemical potential of sulphur is needed to synthesize the oxysulfide. So, it is very difficult to prepare heavy RE oxysulfides in an one-pot soft chemistry rote. Post annealing treatment is necessary to form the Y_2O_2S phase and increase the crystallinity. But, such rigorous reation conditions tend to result in aggregates of nanoparticles and difficulty in controlling the particle size and dispersity. Therefore, the synthesis of heavy RE oxysulfides with high crystallinity still remains a challenge for researchers to date. Yan et al reported a synthesis of Y_2O_2S:Eu nanoplates through thermolysis method, but the preparation demands use of H_2S gas and acetylacetonates in an oxygen-free environment, the crystallinity of product is relatively low.[11]

In this paper, the heavy RE oxysulfide Y_2O_2S has been prepared through a solvothermal reaction method. Ethanediamine and sulphur powder are used as the main solvent and sulphur source to get a higher chemical potential. If PVP are used as capping agents, the monodispersed Y_2O_2S nano-sheets aggregates are obtained. Furthtermore, the amout of sulphur powders also play an important role in controlling the multi-morphologies. Y_2O_2S nano-particles evolve from ultra-thin nanosheets, flower-like structures to solid nano-spheres, with increasing the amout of sulfur. The rare earth doped samples show good luminescent properties without post-calcination treatment. As examples, the luminescent properties of singly doped Eu^{3+} and codoped Er^{3+} ,Yb^{3+} heavy rare earth oxysulfide Y_2O_2S are investigated.

2 Experimental

2.1 Materials

Yttrium acetate ($Y(CH_3COO)_3·4H_2O$) (99.99%) was purchased from Shanghai Diyang Chemicals, the rare-earth nitrates, including $Eu(NO_3)_3·6H_2O$ (99.9%) , $Er(NO_3)_3·6H_2O$ (99.9%), $Yb(NO_3)_3·6H_2O$ (99.9%) and other chemicals (analytical grade purity) were purchased from Aladdin and used without any further purification.

2.2 Methods

In a typical procedure, 0.67 mmol $Y(CH_3COO)_3·4H_2O$ was added into 5 ml absolute ethanol and dissolved completely. Then, 2g PVP (K29–32) was slowly added into the above solution. After vigorous stirring for 30 min, the above solution was drop wise added into 30 ml ethylenediamine solution containing 0.205 g sulfur powder (99.99%). The prepared solution was vigorously stirred for another 30 min. Then it was transferred to a 50 ml Teflon-lined stainless autoclave and heated at 250 °C for 24 h. For the luminescent samples, a certain amount of rare-earth nitrates including $Eu(NO_3)_3$·$6H_2O$, $Er(NO_3)_3·6H_2O$ and $Yb(NO_3)_3·6H_2O$ was added together with $Y(CH_3COO)_3·4H_2O$. The ambient temperature was around 25 °C.

2.3 Characterization

The X-ray powder diffraction (XRD) pattern was recorded using a Japan Regaku D/max çA X-ray diffractometer equipped with graphite monochromatized Cu Kα radiation (λ = 1.5418 Å) irradiated at a scanning rate of 4° min^{-1}. The field-emission scanning electron microscopy (FESEM) images were obtained using a JEOL JSM-7500F microscope operated at an acceleration voltage of 15 kV. A JEOL JEM-200CX microscope operating at 160 kV in the bright-field mode was used for transmission electron microscopy (TEM). The selected area electron diffraction (SAED) pattern was performed on a JEOL JEM-2010 electron microscope operating at 200 kV. The photo-excitation (PLE) and photo-luminescence (PL) spectra were measured using a Varian spectrometer and performed at room temperature. Upconversion (UC) spectra were recorded on a Varian spectrometer equipped with an external power-controllable 980 nm semiconductor laser (Beijing Viasho Technology Company, Beijing, China) as the excitation source.

3 Results and discussion

3.1. Phase Identification and Morphology

Fig.1 shows the XRD patterns of the products prepared at different temperatures for 16 h. The result shows that XRD pattern of sample prepared at 180 °C exhibits a different pattern compared with the JCPDS card 24-1424 of Y_2O_2S, we believe this product should be YOOH according to the JCPDS card 20-1413 of YOOH. When the temperature increases above 200 °C, the clear XRD peaks are well matched with the hexagonal Y_2O_2S phase.

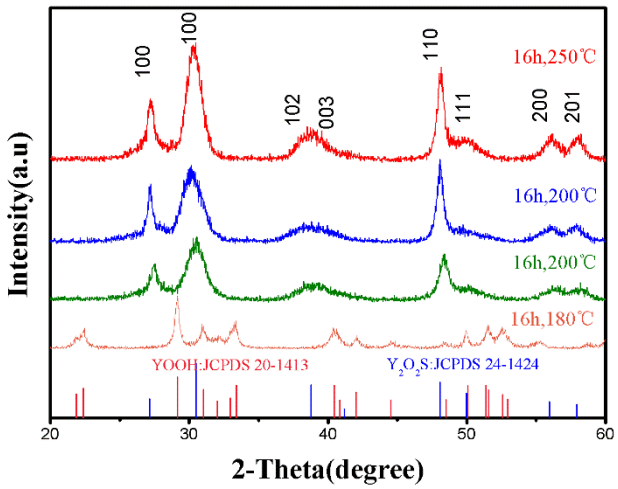

Fig.1 XRD patterns of the Y_2O_2S samples obtained after different solvothermal treatment temperature of 180, 200, 220, 250 °C for 16h

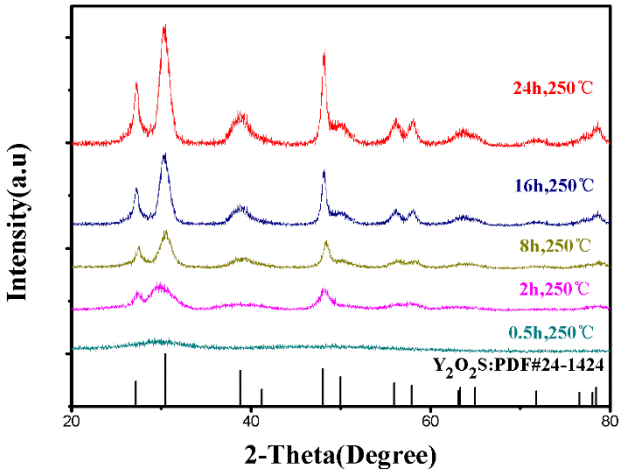

Fig.2 XRD patterns of the Y_2O_2S samples obtained after different solvothermal treatment time of 0.5, 2, 8, 16, 24 h for 250 °C

To investigate the growing process, the XRD patterns of products collected after different solvothermal treatment times of 0.5, 2, 8, 16 and 24 h with other parameters being constant are shown in Fig.2. The products present a broad band after 0.5 h of reaction, indicating it is amorphous and has a low degree of crystallinity. After 2 h or more time of treatment, the peaks are clear and well indexed as the JCPDS 24-1424 Y_2O_2S phase. The XRD results show that the hexagonal Y_2O_2S phase is prepared directly in solvothermal reaction system. As we know, it is difficult to obtain lanthanide oxysulfides, especially heavy rare earth oxysulfides, through some soft synthetic method such as solvothermal reaction and precipitation, because the hard Lewis acid Ln^{3+} doesn't preferentially bind to the soft Lewis base S^{2-}.[11]

In order to solve this problem, we have tried to increase the reaction activity of S^{2+} ions. Ethanediamine and sulphur powder are used as the main solvent and sulphur source to get a higher chemical potential. In the dissolution, a large amount of sulfur forms a complex with ethanedimine and the sulfur ring (S_8) is

changed into sulfur chains (-S-S-). As the temperature is increased, the sulfur polyanions, e.g. S_6^{2-}, S_4^{2-}, can be produced. These polyanions are not stable at high temperature and dissociate, from which required S^{2-} ions are released. The newly produced S^{2-} in high concentration overcome the low affinity of S^{2-} with Y^{3+} to a great extent. As a result, Y_2O_2S could be synthesized directly in this solvothermal reaction system with a relatively low temperature and higher crystallization compared with other Y_2O_2S samples obtained through soft synthetic method reported before.

In addition, ethanol is used as secondary solvent in this method to improve the solubility of the Y $(CH_3COO)_3 \cdot 4H_2O$ and the surfactant. The amount of ethanol should be controlled less than 5 ml in a 40 ml solvent in total. This ratio is quite lower than the synthesis of Gd_2O_2S reported by us before,[12] this phenomenon can be explained that the synthesis of heavy RE element yttrium oxysulfide needs a higher S^{2-} concentration to offer enough sulfur chemical potential.

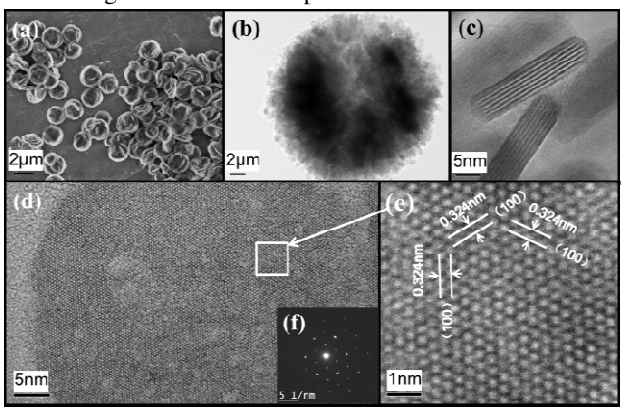

Fig.3 (a): FESEM of monodisperse Y_2O_2S nano-aggregates; (b)–(e): High and low magnification TEM images of Y_2O_2S nano-aggregates; Inset (f) is the SAED pattern.

The morphology of a typical Y_2O_2S nano-aggregates sample is shown in Fig. 3. As shown in Fig 3(a), uniform plate-like aggregates on a large scale are synthesized. The sample shows good dispersibility and a uniform diameter of 2 μm. Detailed observation characterization is shown in Fig. 3 (b~e) by TEM. In Fig. 3(b), it's implied that the plate-like aggregates consisted of nano sheets. From the amplification of the aggregates' edge in Fig.3(c), it's found that the diameter of nano-sheet is 30~50 nm and the thickness is 6~8 nm. Another angle of the nanosheet is shown in Fig. 3(d), an enlarged HRTEM of the selected area in Fig. 3(d) is shown in Fig. 3(e), the lattice fringes image matches well with characteristics of the hexagonal Y_2O_2S crystal, the d spacing of 0.324 nm corresponds to the distance between (100) planes. The inset Fig.3 (f) shows the SAED taken along the [001] zone axis, and a regular hexagonal diffraction pattern indicated that the sample has a hexagonal crystal structure. It can be concluded that nano sheet grows along the [100] crystallographic direction and enclosed by ±(001) facets. This phenomenon is ascribed to the orientation function of the ethanediamine.

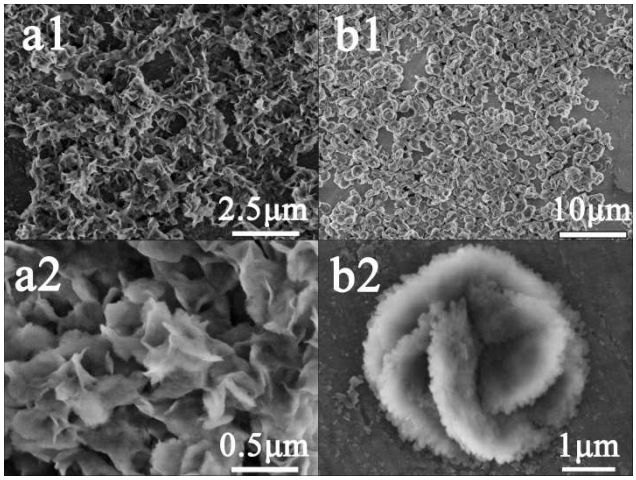

Fig.4 FESEM of the Y_2O_2S samples obtained from (a1,a2) without PVP; (b1, b2) with 2g PVP with the same solvothermal treatment time at 250°C for 24h

The dispersion effect of using PVP as surfactant is shown in Fig. 4. When no surface active agent is used, the product is amorphous cross-linked network structure shown in Fig. 4(a1, a2), but it's obviously consisting of curved nano sheet with a very thin thickness of below 10 nm. When 2 g PVP is used as surfactant, it's clearly implied that Y_2O_2S nano sheet shows an orientation of aggregation. The existence of PVP doesn't change the nanoscale sheet morphology of Y_2O_2S. The selective adsorption on the certain crystal plane of PVP is not as effective as ethanediamine. The viscosity of the solution system is increased by PVP, the cross-linked network structure is unable to be formed because of the barrier effect. The aggregation of nanoscale sheet Y_2O_2S is limited within a small range.[13] Firstly the nanoscale sheet assembles into larger lamellar structure, then uniform micro-plate structure is assembled. After all, the homogeneity and dispersion of the Y_2O_2S nano-aggregates are enhanced efficiently by using PVP as surfactant.

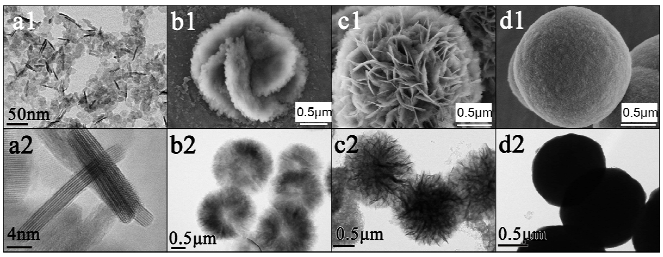

Fig.5 FESEM and TEM of the Y_2O_2S samples obtained from different initial Sulfur concentration (a1, a2):0.08 M; (b1, b2):0.16M; (c1c2):0.4M; (d1, d2):0.8M at 250 °C for 24 h

Fig. 5 shows different morphology results by simply changing the concentration of sulfur powder when other parameters being constant. When the concentration of sulfur powder is as low as 0.08 M, Fig. 5(a1, a2) shows that Y_2O_2S nano-sheets are obtained, and the thickness and diameter are ~5 nm and ~20 nm, respectively. With the sulfur concentration increased to 0.16M, Y_2O_2S nano-sheets are assembled into a

plate like structure with a diameter of ~2 μm, shown in Fig. 5(c1, c2). When the sulfur concentration is further increased to 0.4 M, much more Y_2O_2S nano-sheets are assembled into a flower like structure with a diameter of ~2 μm. It is easy to find that the sheets structure is maintained, if the sulfur concentration is not too high. However, when the concentration of sulfur powder reaches 0.8 M, the morphology and structure of Y_2O_2S product change greatly. Sheets structure disappears and the morphology turns into nano particles-assembled solid spheres with a diameter of 1.5 μm.

According to the Y_2O_2S morphology under different reaction conditions, we conclude a morphology control rule in this reaction system as shown in Fig. 6. In the initial stage of reaction, small hexagonal particles of Y_2O_2S are obtained after nucleation and crystal growth under the oriented effect of the solvent and surfactant. If the concentration of sulfur powder is too high (0.8 M), nucleus number is relatively higher, the growth speed of small particles is slower than accumulation reunion's, therefore the particles will aggregate into dense sphere structure.

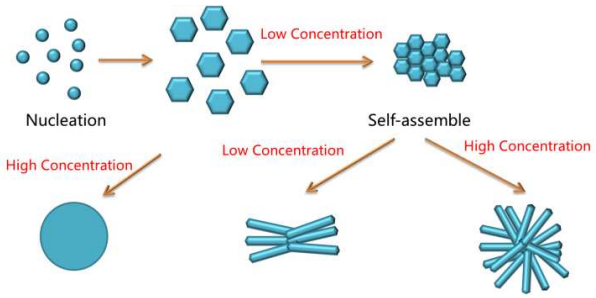

Fig.6 Schematic illustration of the Y_2O_2S nano-aggregates growth model.

On the other hand, if the concentration of sulfur powder is very low (0.08 M), nucleus growth occupied the dominant position, hexagonal particles will assembled into nano sheet with a thickness of ~5nm, because this condition is difficult to control in the solvothermal system, the reunion phenomenon will appear to some extent. When the concentration of sulfur powder is in the middle value, nano sheet will be assembled into larger size nanosheet, the size growth will compete with assembling, when the concentration of sulfur powder is relatively lower, size growth will be in the first place and micrometer-grade plate assembled with larger nanosheets will be obtained. On the contrary, micrometer grade flower-like structure assembls with smaller nanosheets will be obtained.

3.2. Photoluminescence Properties

Due to low phonon energies, low symmetry, outstanding chemical stability and nontoxicity, Y_2O_2S is an ideal luminescence host which is used in CRT imaging, cathode ray luminescence, upconversion phosphor and many other areas.

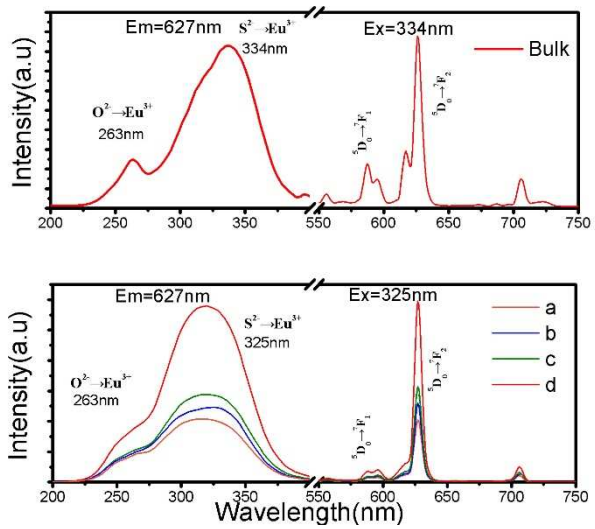

Fig.7 Excitation and emission spectra of nano-aggregates/bulk Y_2O_2S:0.01Eu^{3+} with the same doped rate. The a, b, c, d represents nano-aggregates of different morphology: nano sheet, sheet-assembled plate, sheet-assembled flower, nano-assembled sphere, respectively.

In this paper, Eu^{3+} is doped in Y_2O_2S nano-aggregates with the best doping rate of 1%. Room temperature excitation spectra of Y_2O_2S:Eu^{3+} nano-aggregates and bulk Y_2O_2S:Eu^{3+} synthesized at 1050 °C for 4h, monitored at 627 nm, are shown in Fig. 6. As we know, the excitation band from 250 to 300 nm can be ascribed to O^{2-} to Eu^{3+} charge transfer and the broad excitation band above 300 nm is ascribed to S^{2-} to Eu^{3+} charge transfer in this system.[14] The excitation band width exhibits a broad trend in Y_2O_2S:Eu^{3+} nano-aggregates compared with the bulk sample, this may be ascribe to the increase of defects and surface effect of nano materials. At the same time, the excitation band above 300 nm shows a blue-shift of 9 nm in nano-aggregates, the similar phenomenon is observed in several references.[9] Yan and co-workers synthesized Y_2O_2S:Eu^{3+} through thermolysis method, it's found that the peak of excitation band is 251 nm with several lower peaks above 300 nm because of the specific nano plate structure, S^{2-} to Eu^{3+} charge transfer is not so effective. In this paper, Y_2O_2S:Eu^{3+} nano-aggregates are consist of nano sheet, since the nano sheet is terminated by Y^{3+} on both (001) facets, the S^{2-} ion on the surface is not as many as that in bulk sample, as a result, the peak above 300 nm shifted to 325 nm in nano-aggregates. The main emission peaks are ascribed to the Eu^{3+} ion transition from ^5D_J (J = 0, 1) to ^7F_J (J = 1–4). The Red/Orange value is much higher in the nano-aggregates material and the emission peaks intensity (Intensity=20.7) decrease, compared to the bulk sample (Intensity=100). The lower crystal field symmetry at the surface is considered to be the main origin of the unusual phenomenon.[10] It is already known that a blue shift in the Eu^{3+} ligand charge transfer band can lead to enhancement in the $^5D_0 \rightarrow {}^7F_2$ transition.[15] As a result, the ratio of peaks intensity responding to $^5D_0 \rightarrow {}^7F_2$ transition and $^5D_0 \rightarrow {}^7F_1$ or other transition is much higher in Y_2O_2S:Eu^{3+} nano-aggregates compared to bulk sample.

Excitation and emission spectra of different morphologies are also shown in Fig. 7. The sphere nano-aggregate $Y_2O_2S:Eu^{3+}$ shows the strongest peaks intensity while the other three morphologies of $Y_2O_2S:Eu^{3+}$ show the similar intensity. This phenomenon can be ascribed to the sphere nano-aggregates have the lowest surface defects and highest light absorption for the sphere structure. While all other three morphologies consisted of similar nano sheets which have a similar luminescence properties, but the flower-like nano-aggregates is closer to the sphere structure，the nano sheet exposes more defects, the former has a relatively strong intensity and the latter's is the lowest.

The upconversion luminescent properties of Yb^{3+}/Er^{3+} doped Y_2O_2S is studied by adjusting the doping concentration. The sphere morphology of Y_2O_2S nano-aggregates is used as the host. The emission spectra when excited with 980nm pumped laser is shown in Fig. 8. By adjusting the doping ratio of Er^{3+}/Yb^{3+}, the green/red luminescence ratio can be adjusted

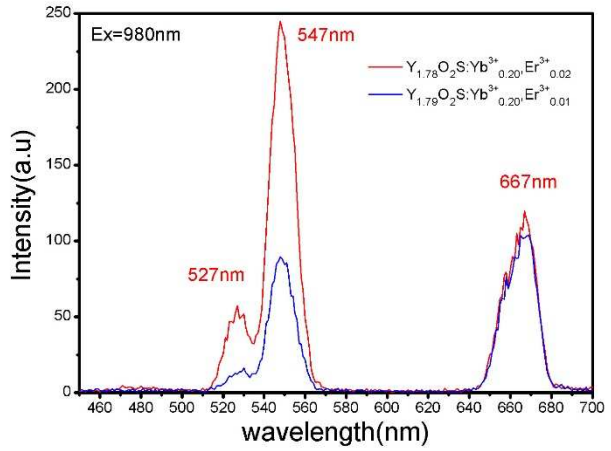

Fig. 8 upconversion luminescence properties of Yb^{3+}/Er^{3+} doped Y_2O_2S nano-aggregates with varying doping concentration under 980nm laser excitation.

effectively. With the increase of Er^{3+} ion concentration, the green light component increased.

The relationship between peak intensity and the laser pump power can be presented in formula of $I\alpha P^n$（n≥2）, therefore the photon number in one conversion process can be calculated. As logarithmic plot shown in Fig. 9, for 527nm ($^2H_{11/2}\rightarrow{}^4I_{15/2}$), 547nm ($^4S_{3/2}\rightarrow{}^4I_{15/2}$) and 667nm ($^4F_{9/2}\rightarrow{}^4I_{15/2}$), the slopes are 1.84, 1.82 and 1.89 respectively which prove that all the three conversion process absorb two low-energy photons and emit one high-energy photon.

Fig. 10 shows the energy level transition process of upconversion of Yb^{3+}/Er^{3+} doped Y_2O_2S. There are two ways for Er^{3+} ions to be inspired to the excited state $^4I_{11/2}$ from the ground state $^4I_{15/2}$: the first way is the ground state absorption (ESA) of Er^{3+} ion, and the second way is through the process of energy transfer (ETU) from Yb^{3+} ions:$Er^{3+}(^4I_{15/2})$ + $Yb^{3+}(^2F_{5/2})$ $\rightarrow Er^{3+}(^4I_{11/2})$ + $Yb^{3+}(^2F_{7/2})$ which refers to that the energy absorbed by Yb^{3+} ion at the excited state are transmitted to the neighboring Er^{3+} ion because the energy is consistent. Obviously, the latter way dominated, because the absorption of Er^{3+} ions is poor at 980 nm excitation light source compared to the absorption intensity of Yb^{3+} ions. When Er^{3+} ion reach excited state $^4I_{11/2}$, it can be excited to $^4F_{7/2}$ level by another ETU process or ESA process. The Er^{3+} ion at $^4F_{7/2}$ level will get to $^2H_{11/2}$, $^4S_{3/2}$ and $^4F_{9/2}$ level through radiationless relaxation, and finally transit back to ground state level to emit the corresponding green light (527 nm, 547 nm) and red light (667 nm). This process is also consistent with the the upconversion processes of two photon calculated before.

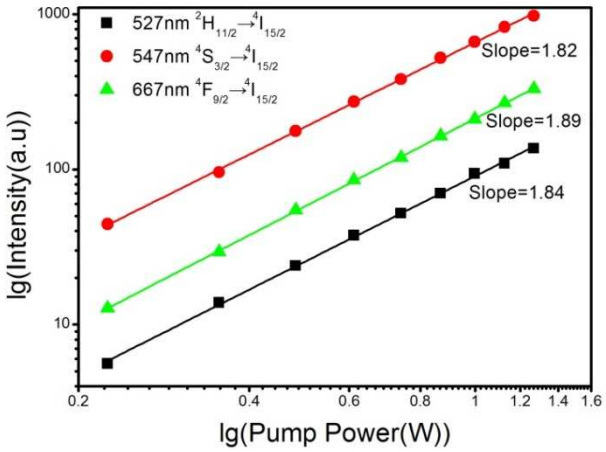

Fig. 9 Power dependence of UC intensity (527,547,667nm) of Y_2O_2S:10%Yb^{3+}, 1%Er^{3+} nano-assembled spheres

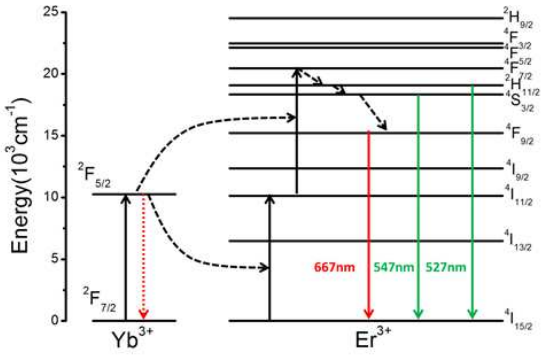

Fig. 10 Energy Level diagram of Yb3+ and Er3+ and the possible ESA and ETU in UC process.

4 Conclusions

In summary, the heavy rare earth oxysulfide Y_2O_2S is directly synthesized by a facile and mild solvothermal reaction method for the first time. Ethanediamine, which dissolves sulphur powder and releases active S^2 ions in high concentration, is used to overcome the low affinity of S^{2-} ion with Y^{3+} ion. By simply adjusting the amount of initial sulfur powder, the morphology and assembled structure can be well

controlled. The luminescent properties of Eu^{3+} doped Y_2O_2S with different morphology are studied. The sphere nano-aggregates show the strongest emission intensity because of less surface defects. Under 980 nm laser excitation, $Y_2O_2S:Yb^{3+},Er^{3+}$ nano-phosphors exhibit a tunable emission, shifting from greenish-yellow to orange-yellow, by increasing Yb^{3+}/Er^{3+} ratio. The solvothermal reaction method reported in this paper is also helpful for the synthesis of other lanthanide oxysulfide NCs.

Acknowledgements

This work is supported by Shanghai Science & Technology Committee (12521102501), Shanghai Educational Committee (11ZR1426500), Innovation Program of Shanghai Municipal Education Commission (14ZZ127), PCSIRT(IRT1269), the Program of Shanghai Normal University (DZL124) and Academic Leaders Training Program of Pudong Health Bureau of Shanghai (Grant No. PWRd2011-09)

Notes and References

# Equal contribution as the first author
a The Education Ministry Key Laboratory of Resource Chemistry and Shanghai Key Laboratory of Rare Earth Functional Materials, Department of Chemistry, Shanghai Normal University, Shanghai 200234, People's Republic of China
b Physics and Chemistry Test Lab, Shanghai Pudong New Area Center for Disease Control & Preverntion, Shanghai 200136, People's Republic of China
* Corresponding Author: liujie@shnu.edu.cn, xibinyu@shnu.edu.cn, mzhan@pdcdc.sh.cn

† Electronic Supplementary Information (ESI) available. See DOI: 10.1039/b000000x/

1. L. Ozawa and M. Itoh, *Chemical Reviews*, 2003, **103**, 3835-3856.
2. D. Liu, C. e. Cui, P. Huang, L. Wang and G. Jiang, *Journal of Alloys and Compounds*, 2014, **583**, 530-534.
3. S. Deng, Z. Xue, Y. Liu, B. Lei, Y. Xiao and M. Zheng, *Journal of Alloys and Compounds*, 2012, **542**, 207-212.
4. X. Liu, L. Pan, J. Li, K. Yu, Z. Sun and C. Q. Sun, *Journal of Colloid and Interface Science*, 2013, **404**, 150-154.
5. Y. Song, Y. Huang, L. Zhang, Y. Zheng, N. Guo and H. You, *RSC Advances*, 2012, **2**, 4777-4781.
6. Y. Song, H. You, Y. Huang, M. Yang, Y. Zheng, L. Zhang and N. Guo, *Inorganic Chemistry*, 2010, **49**, 11499-11504.
7. F. Zhao and S. Gao, *Journal of Materials Chemistry*, 2008, **18**, 949-953.
8. F. Zhao, M. Yuan, W. Zhang and S. Gao, *Journal of the American Chemical Society*, 2006, **128**, 11758-11759.
9. Y. Ding, J. Gu, J. Ke, Y.-W. Zhang and C.-H. Yan, *Angewandte Chemie-International Edition*, 2011, **50**, 12330-12334.
10. Y.-P. Du, Y.-W. Zhang, L.-D. Sun and C.-H. Yan, *Journal of the American Chemical Society*, 2009, **131**, 3162-3163.
11. J. Gu, Y. Ding, J. Ke, Y. Zhang and C. Yan, *Acta Chimica Sinica*, 2013, **71**, 360-366.
12. J. Liu, H. Luo, P. Liu, L. Han, X. Zheng, B. Xu and X. Yu, *Dalton Transactions*, 2012, **41**, 13984-13988.
13. K. Zhang, D. Zhang, J. Liu, K. Ren, H. Luo, Y. Peng, G. Li and X. Yu, *CrystEngComm*, 2012, **14**, 700-707.
14. Q. Dai, H. Song, M. Wang, X. Bai, B. Dong, R. Qin, X. Qu and H. Zhang, *The Journal of Physical Chemistry C*, 2008, **112**, 19399-19404.
15. G. Blasse, *Structure and Bonding*, 1976, **26**, 43-79.

